Regional Climate Impacts of the Northern Hemisphere Annular Mode

David W. J. Thompson, *et al.*

Science **293**, 85 (2001);
DOI: 10.1126/science.1058958

over more extended regions. In this regard, composite β pulses with a properly designed functional dependence of rotation amplitude on ω_1 should lead to improved refocosing for general of profiles.

The extension of these principles to multidimensional spectroscopy is straightforward, and Fig. 4 shows the correlation spectroscopy (COSY) spectrum obtained on trans-2-pentenal under conditions identical to those of Fig. 2 with the field gradients applied. Cross peaks indicating *J*-coupled proton spins are still recognizable even though the field inhomogeneity is sufficient to completely erase any spectroscopic information. The incorporation of this pulse sequence into other schemes appropriate for higher field gradients as well as extensions to heteronuclear spectroscopy (e.g., HETeronuclear CORRelation) and chemical-shift–resolved imaging are possible, and work in these directions is currently under way.

We not that the full spectroscopic information of a sample can still be obtained if a period of free evolution under a static field gradient is followed by another period with the field gradient reversed. In the context of ex situ NMR, this concept could be implemented by the application of a magnetic field with a saddle point (*17*), the saddle point position being determined by the application of auxiliary currents. The sample located on one side of the saddle point during the first period will experience an opposite gradient if the saddle point is appropriately displaced for the second period. This procedure represents an extension of the sequence discussed above, now based on the degree of correlation attainable with static field matching on both sides of the saddle point. Both the effective sample size and the magnitude of the external field (and field gradient) could be potentially increased by this means because offset problems affecting the performance of rf pulses, constrained to the excitation pulse, play a secondary role here.

Finally, we mention a possible extension of the field variation concept that involves the use of several coils to generate a magnetic field spinning at the magic angle (*18*, *19*) with respect to static ex situ samples. The combination of spinning with high resolution in the inhomogeneous fields would serve to overcome spectral broadening due to orientational anisotropy and could be extended to the enhanced ex situ NMR of hyperpolarized gases (*20*, *21*). Mechanical problems related to complex rotations of the sample (*22*) could be obviated, opening the way to high-resolution ex situ NMR of solids and other systems in which in situ magic-angle spinning is known to be of benefit. Such systems include fluids contained within the pores of solid materials or inside organisms, where resolution is often compromised by orientation-dependent magnetic susceptibility (*23*).

References and Notes

1. J. J. H. Ackerman, T. H. Grove, G. G. Wong, D. G. Gadian, G. K. Radda, *Nature* **283**, 167 (1980).
2. J. F. Stebbins, I. Farnan, *Science* **245**, 257 (1989).
3. S. Frank, P. C. Lauterbur, *Nature* **363**, 334 (1993).
4. M. D. Hürlimann, D. D. Griffin, *J. Magn. Reson.* **143**, 120 (2000).
5. B. Blümich *et al.*, *Magn. Reson. Imag.* **16**, 479 (1998).
6. D. P. Weitekamp, J. R. Garbow, J. B. Murdoch, A. Pines, *J. Am. Chem. Soc.* **103**, 3578 (1981).
7. J. J. Balbach *et al.*, *Chem. Phys. Lett.* **277**, 367 (1997).
8. L. D. Hall, T. J. Norwood, *J. Am. Chem. Soc.* **109**, 7579 (1987).
9. W. Richter, S. Lee, W. S. Warren, Q. He, *Science* **267**, 654 (1995).
10. A. Jershow, *Chem. Phys. Lett.* **296**, 466 (1998).
11. A. Sharfenecker, I. Ardelean, R. Kimmich, *J. Magn. Reson.* **148**, 363 (2001).
12. I. Ardelean, R. Kimmich, A. Klemm, *J. Magn. Reson.* **146**, 43 (2000).
13. M. H. Levitt, *The Encyclopedia of NMR* (Wiley, London, 1997), pp. 1396–1411.
14. Point-by-point acquisition with a sequential increment of the β-pulse length is conceivable as well. However, as in the Carr-Purcell train, incomplete refocusing due to diffusion is best suppressed by keeping the free evolution time sufficiently short.
15. Closer examination of Fig. 2C shows that the chemical shift scale is slightly enhanced with respect to the conventional spectrum, an effect that arises from the evolution of the nuclear magnetization under the field offset during the composite π/2 pulses. This renders the effective dwell time slightly longer than the free evolution period τ_{dw} used for the Fourier transformation. A correction can be applied by simply rescaling the shift scale. Undesired offset-induced evolution during the rf pulses also leads to spectral artifacts that distort neighboring peaks around the irradiation frequency. However, the results in Fig. 2C show that these effects can be overcome to a great extent by a phase alternation on the composite z-rotation pulses at each step of the pulse train (see Fig. 3B). Further improvement can be obtained by tuning the rf toward lower frequencies (corresponding to spins located farther away from the coil). If the rf field is high enough, this ensures that most nuclei contributing substantially to the signal experience a reduced offset effect during the β pulse.
16. The gradient can be further increased if the composite π/2 pulses are replaced by single pulses of adjustable length. When this length matches the 90° condition for on-resonance nuclei, a highly spatially selective excitation occurs that still provides extremely sharp spectra, with a correspondingly diminished sensitivity.
17. R. L. Kleinberg, A. Sezginer, D. D. Griffin, M. Fukuhara, *J. Magn. Reson.* **97**, 466 (1992).
18. E. R. Andrew, A. Bradbury, R. G. Eades, *Nature* **182**, 1659 (1958).
19. E. R. Andrew, R. G. Eades, *Disc. Faraday Soc.* **34**, 38 (1962).
20. M. S. Albert *et al.*, *Nature* **370**, 199 (1994).
21. G. Navon *et al.*, *Science* **271**, 1848 (1996).
22. B. F. Chmelka, A. Pines, *Science* **246**, 71 (1989).
23. T. M. de Swiet, M. Tomaselli, M. D. Hürlimann, A. Pines, *J. Magn. Reson.* **133**, 385 (1998).

24. We thank J. D. Walls for fruitful discussions and A. H. Trabesinger for kindly reviewing the manuscript. This work was supported by the Director, Office of Science, Office of Basic Energy Sciences, Materials Sciences Division, of the U.S. Department of Energy under contract DE-AC03-76SF00098. C.A.M. acknowledges Consejo Nacional de Investigaciones Científicas y Tecnológicas, Argentina, and H.H. thanks the Humboldt Foundation for support through postdoctoral fellowships.

10 April 2001; accepted 30 May 2001

Regional Climate Impacts of the Northern Hemisphere Annular Mode

David W. J. Thompson[1]* and John M. Wallace[2]

The Northern Hemisphere annular mode (NAM) (also known as the North Atlantic Oscillation) is shown to exert a strong influence on wintertime climate, not only over the Euro-Atlantic half of the hemisphere as documented in previous studies, but over the Pacific half as well. It affects not only the mean conditions, but also the day-to-day variability, modulating the intensity of mid-latitude storms and the frequency of occurrence of high-latitude blocking and cold air outbreaks throughout the hemisphere. The recent trend in the NAM toward its high-index polarity with stronger subpolar westerlies has tended to reduce the severity of winter weather over most middle- and high-latitude Northern Hemisphere continental regions.

The NAM is a planetary-scale pattern of climate variability characterized by an out-of-phase relation or seesaw in the strength of the zonal flow along ~55° and 35°N and accompanied by displacements of atmospheric mass between the Arctic basin and the mid-latitudes centered ~45°N (*1*–*4*). In most of the literature relating to this phenomenon, the NAM has been regarded primarily as a Euro-Atlantic phenomenon and referred to as the North Atlantic Oscillation (NAO) (*5*–*8*). Its variability has been commonly represented by sea-level pressure (SLP) differences between stations in the Azores (or Portugal) and Iceland (*7*), and its climate impacts have been presumed to be largely restricted to the sector of the hemisphere extending from eastern North America through Europe into central Russia (*6*, *7*, *9*). Here, we demonstrate that

[1]Department of Atmospheric Science, Colorado State University, Fort Collins, CO 80523, USA. [2]Department of Atmospheric Sciences, University of Washington, Seattle, WA 98195, USA.

*To whom correspondence should be addressed. E-mail: davet@atmos.colostate.edu

the impacts of the NAM are clearly evident at virtually all longitudes.

The analysis is based on 40 years (1958–1997) of daily-mean data from the NCEP/NCAR Reanalysis (National Centers for Environmental Prediction and the National Center for Atmospheric Research) together with selected station data (*10*). Variability in the NAM is represented by the leading principal component (PC) time series of the monthly mean Northern Hemisphere (NH) (20° to 90°N) SLP field (*4*), which captures the hemispheric scale features of the NAM more faithfully than regional station-based indices (*8*). All results are based on the winter season, defined here as January to March (JFM) (*11*), when the tropospheric and lower stratospheric circulations are coupled (*4*, *12*) and the variability of the NAM is largest (*4*). The high (low) index polarity of the NAM is defined as anomalously strong (weak) subpolar westerlies. High- and low-index days during JFM from 1958–1997 are defined as days on which anomalies in the daily NAM index exceed one standard deviation (SD) in absolute value (*13*). About one-third of all days, 1958–1997, correspond to either the high- or the low-index polarity of the NAM (Fig. 1 and Table 1). The large sample size afforded by our use of daily data enables us to document the signature of the NAM not only in mean climate, but also in the frequency of occurrence of a representative selection of "significant weather events" throughout the NH, i.e., "cold events" in which daily minimum temperature drops below a specified threshold corresponding to 1.5 SD below the local JFM seasonal mean, frozen precipitation, blocking (*14*) in the three subarctic regions where it is observed to occur most frequently, and high winds and wave heights. All the results presented in Tables 2 and 3 are statistically significant at the 95% confidence level or higher on the basis of a Monte Carlo test (*15*) and were found to be highly reproducible in data for nearby stations.

Composite maps of surface air temperature (SAT) and SLP for the high- and low-index polarities of the NAM (Fig. 2) reveal the most pronounced differences over Europe, but substantial differences are observed over North America and the Arctic basin as well. High-index conditions are characterized by westerly geostrophic surface winds along 55°N and transpolar flow from Russia toward Canada, whereas low-index conditions are marked by cold anticyclones centered over central Canada and Russia and an anticyclonic surface circulation throughout the Arctic basin. High-index days are, on average, ~5°C warmer over much of the midwestern United States, central Canada, and Europe. The 0°C isotherm runs through the southern

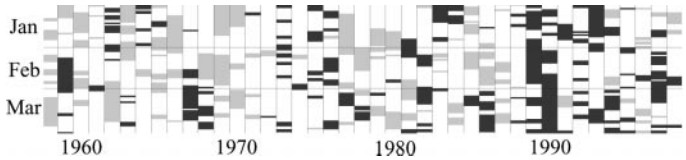

Fig. 1. The index of the NAM during January–March (JFM), 1958–1998. High index days (dark shading) and low index days (gray shading) are defined as days on which the daily NAM-index exceeds ±1 SD about the JFM mean, and together account for a total of ~1/3 of all days during JFM (Table 1).

Table 1. Numbers of high and low NAM–index days during JFM (*11*) for the periods indicated.

	Total JFM days	High NAM days	Low NAM days
1958–1997	3600	597	595
1958–1967	900	104	209
1988–1997	900	273	44

Table 2. Significant weather events associated with high and low NAM–index days. Total, the total number of events; NAM+ and NAM−, the number of events falling on high- and low-index days, respectively; ΔT_{mean}, the ratio attributable to shifts in mean temperature induced by fluctuations in the NAM (*19*); Trend NAM and Trend Gl. Wm., the estimated trends in the frequency of occurrence of cold events between 1958–1967 and 1988–1997 that are attributable to trends in the frequency distribution of the NAM and global-mean temperature, respectively (*28*). All results for NAM+ and NAM− exceed the 95% confidence level (*15*). Results are based on daily data, JFM 1958–1997, except buoy data, which are available 1981–1997.

Event type and location	Total	NAM+	NAM−	ΔT_{mean}	Trend NAM	Trend Gl. Wm.
Cold daily minimum temperature (*29*)						
<–15°C in Juneau, AK	352	32	84	1:1.5	–23%	–10%
<–18°C in Chicago, IL	330	29	84	1:2.3	–31%	–9%
<3°C in Orlando, FL	267	31	68	1:2.3	–29%	–12%
<–3°C in Paris, France	298	23	97	1:2.7	–39%	–15%
<–29°C in Novosibirsk, Russia	268	21	85	1:2.6	–31%	–7%
<–19°C in Beijing, China	212	21	55	1:1.9	–17%	–10%
<–1°C in Tokyo, Japan	304	20	93	1:1.8	–37%	–21%
Frozen precipitation (*29*)						
>Trace snow in Dallas, TX	56	1	17			
>Trace snow in Memphis, TN	130	7	36			
>Trace snow in Atlanta, GA	67	4	19			
>5 cm snow in Baltimore, MD	119	11	31			
>0.5 cm snow in Paris, France	182	11	63			
>0 cm snow in Tokyo, Japan	109	8	25			
Winds/waves (*30*)						
>25 knots, Seattle, WA	333	78	27			
>35 knots, Astoria, OR	251	55	20			
Offshore waves >6.5 m, WA	144	30	12			
>30 knots with snow, Boston, MA	206	22	45			
Offshore waves >5 m, MA	122	10	36			
>50 knots, Keflavik, Iceland	276	81	19			
Blocking days (*14*, *31*)						
Alaska (170°E–150°W; 60°N–75°N)	385	53	98			
North Atlantic (50°W–0°; 60°N–75°N)	439	1	225			
Russia (40°E–70°E; 60°N–75°N)	412	29	82			

Table 3. As in Table 2, but for cold events at select stations over the northwestern United States. All results are based on daily station data, JFM 1958–1997.

Event type and location	Total	NAM+	NAM−	ΔT_{mean}	Trend NAM	Trend Gl. Wm.
Cold daily minimum temperature						
<–5°C in Bellingham, WA	218	25	58	1:1.7	–13%	–15%
<–3°C in Portland, OR	271	29	73	1:1.5	–18%	–16%
<–11°C in Yakima, WA	304	38	99	1:1.6	–24%	–12%
<–10°C in Wenatchee, WA	309	39	91	1:1.8	–18%	–12%
<–12°C in Spokane, WA	330	44	92	1:1.6	–14%	–11%
<–11°C in Moscow, ID	306	39	82	1:1.5	–12%	–11%
<–16°C in Missoula, MT	324	41	82	1:1.7	–18%	–10%
<–23°C in Great Falls, MT	304	31	90	1:2.1	–32%	–7%
Frozen precipitation						
>Trace snow in Seattle, WA	146	15	36			
>Trace snow in Portland, OR	135	12	43			

Great Lakes and eastern Europe on high-index days but dips into the Ohio Valley and extends westward into France on low-index days. High-index days are warmer throughout the Barents and Kara Seas, but warm anomalies observed under high-index conditions in buoy data over the western Arctic (*16*) are only weakly apparent. Consistent with previous studies (*7*, *9*, *17*), the contrasting polarities of the NAM are associated with large differences in the distribution of precipitation over Europe and the Middle East; substantial differences are observed over the west coast of North America as well.

Composite maps of 500-hPa height and the SD of band-pass filtered 500-hPa height field (*18*) also reveal pronounced differences throughout the NH (Fig. 3). High-index conditions are marked by increased variance across the North Atlantic stormtrack from northeastern North America to northern Europe and across the North Pacific stormtrack from east Asia into the Pacific Northwest of the United States. Low-index conditions are suggestive of blocking (*14*) in the midtropospheric circulation over both Alaska and the North Atlantic.

The contrasting polarities of the NAM are marked by distinct differences in the frequency distribution of significant weather events throughout the NH, consistent with the results presented in Figs. 2 and 3. Cold events occur with much greater frequency over North America, Europe, Siberia, and east Asia under low-index conditions (Fig. 4, top; Tables 2 and 3), increasing the risk of frost damage and the frequency of occurrence of frozen precipitation events over regions where these events tend to be mainly temperature-limited (Tables 2 and 3). High-index conditions are marked by an increased frequency of occurrence of strong winds over northern Europe and the Pacific Northwest (Table 2). In New England, the juxtaposition of strong winds and snowfall, the hallmark of coastal storms known as "Nor'easters," occurs more frequently under low-index conditions.

The results based on the NCEP/NCAR Reanalysis are in close agreement with those derived from station data throughout most of the United States (the only region for which extensive archives of daily station data exist in the public domain). The only notable exception is over the Pacific Northwest, where the NAM exhibits a much more pronounced signature in the frequency of occurrence of cold events in station data (Table 3) than it does in results based on the Reanalysis (Fig. 4, top). The strength of the linkages in Table 3 attests to the strong influence of the NAM on winter climate over western North America.

The part of the difference in the frequency of occurrence of extreme temperature events that is attributable simply to the shifts in mean temperature induced by fluctuations in the NAM is indicated in the ΔT_{mean} column of Tables 2 and 3 and the bottom panel of Fig. 4 (*19*). The remaining difference is due to changes in the shape of the frequency distribution of temperature. The observed ratios are generally larger and substantially more statistically significant than those expected solely on the basis of a shift in the mean temperature. The additional increment is a reflection of the longer negative tail on the frequency distribution of daily minimum temperature observed under low-index conditions, which is attributable to the increased incidence of high-latitude blocking (Table 2) and associated cold air outbreaks (*14*).

The notion of blocking and cold air outbreaks being orchestrated on a hemispheric scale was anticipated by Namias and collaborators in early investigations of the so-called "zonal index cycle" (*1*), but was abandoned nearly 50 years ago for lack of evidence of statistically significant relations between climate anomalies in the North American and Eurasian sectors (*20*). Most studies since then have tended to focus on more regional phenomena. The relations in Tables 2 and 3 provide renewed support for the relevance of the zonal index (or NAM) paradigm. The fact that the relations in Tables 2 and 3 can be recovered using a NAM index based on data for the Atlantic (60°W-30°E) quadrant of the hemisphere alone (*21*) substantiates our premise that the NAM is a physical mode of variability of the hemispheric circulation and not merely an artifact of using an index derived from hemispheric pressure data or [as in the early zonal index studies of the 1940s (*1*, *2*, *22*)] an index based on zonally averaged data.

The NAM has exhibited a pronounced trend toward its high-index polarity since the late 1960s that is evident in its time series (*3*, *7*, *23*) and is also reflected in the relative numbers of low- and high-index days in different decades (Fig. 1, Table 1). The stronger westerly flow at subpolar latitudes in recent

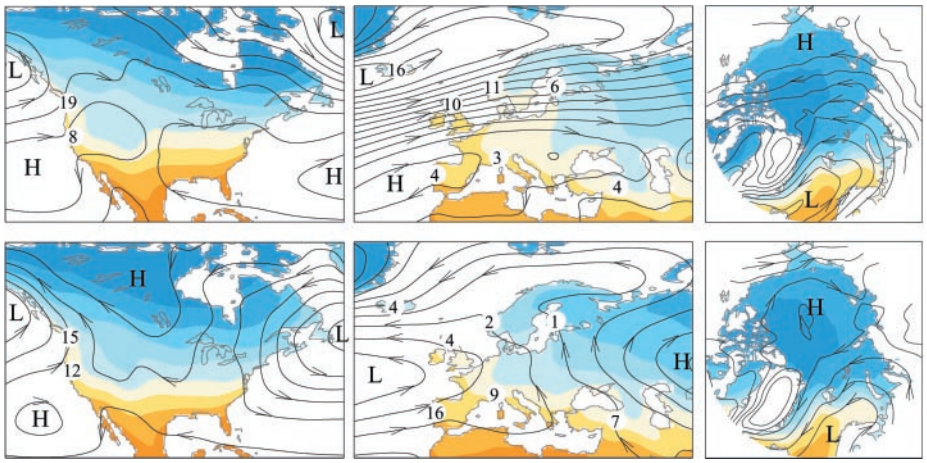

Fig. 2. Composite maps of surface air temperature (shading), sea-level pressure (contours), and precipitation (numbers) for high NAM-index (*top*) and low NAM-index (*bottom*) days based on daily JFM data, 1958–1997, from the NCEP/NCAR Reanalysis (*10*). Contour intervals are 5°C for temperature (blue shades indicate values less than 0°C over North America and Europe and –10°C over the Arctic), and 3 millibars (mb) for SLP (highest contour is 1022 mb over North America and 1025 mb over Europe). Precipitation is in cm/month.

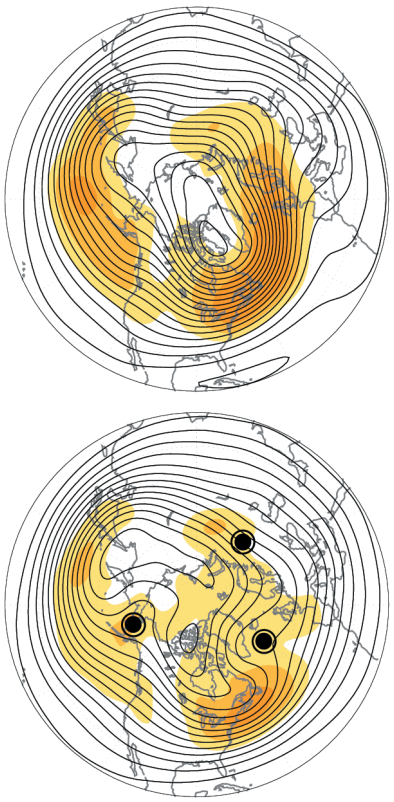

Fig. 3. As in Fig. 2, but for composite maps of 500-hPa height (contours) and the SD of band-pass filtered 500-hPa height field (shading) (*18*). Blocking regions (*14*) used in Table 2 are marked by black dots. Contour intervals are 50 m for 500-hPa height (the lowest contour is 4950 m in the high-index composite and 5150 m in the low-index composite). Shading is drawn for SD values of 50, 60, and 70 m.

years has favored warmer wintertime-mean temperatures across much of the NH high-latitude continents (*23*, *24*), including all of the stations listed in Tables 2 and 3, and a decreased incidence of high-latitude blocking. Milder wintertime mean conditions and a decreased incidence of blocking have both favored a declining frequency of occurrence of cold events. This rate of decline is estimated and compared with that attributable to global warming in the last two columns of Tables 2 and 3. The combined declines attributable to global warming and the trend in the NAM are typically in the 30 to 50% range; at all but one station the decline attributable to the NAM is larger.

The relations documented in this paper illustrate how the natural modes of variability of the climate system modulate not only seasonal mean statistics like temperature and precipitation, but also the frequency of occurrence of weather events that impact human activities. To the extent that these modes are predictable, such relations can be of practical use in applications that involve assessing the risk of such events. A predictive capability already exists for the El Niño–Southern Oscillation phenomenon (*25*), and there is hope that one might eventually be developed for the NAM, exploiting its connection with the wintertime stratospheric circulation (*12*, *26*). Even in the absence of a true predictive capability, knowledge of the observed trend in the NAM toward its high-index polarity can be useful in interpreting recent trends in weather and climate statistics. If this trend proves to be anthropogenic, as suggested by recent climate modeling experiments (*27*), statistics like those presented here may prove useful in making projections of what winters will be like later in this century.

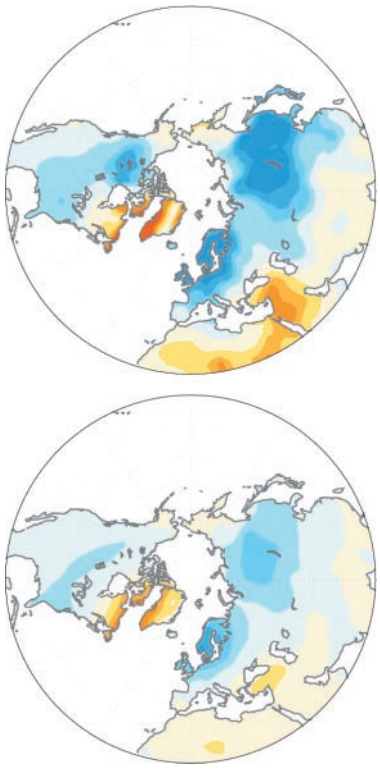

Fig. 4. The signature of the NAM in the frequency of occurrence of cold events (daily minimum temperature <1.5 SD below the climatological mean) based on 6-hourly JFM data, 1958–1997, from the NCEP/NCAR Reanalysis (*10*). (Top) The ratios of the number of cold events in the low NAM–index sample to the number of cold events in the high NAM–index sample. (Bottom) As in the top panel, but for the ratios attributable to shifts in mean temperature (*19*). Shading is drawn for ratios ± 2:1, 3:1, 4:1, and 6:1. Blue shading indicates more cold events under low index conditions. Ratios > ~2:1 exceed the 95% confidence level (*15*).

References and Notes

1. J. Namias, *J. Meteorol.* **7**, 130 (1950).
2. E. N., Lorenz, *J. Meteorol.* **8**, 52 (1951).
3. D. W. J. Thompson, J. M. Wallace, *Geophys. Res. Lett.* **25**, 1297 (1998).
4. _____, *J. Clim.* **13**, 1000 (2000).
5. G. T. Walker, E. W. Bliss, *Mem. R. Meteorol. Soc.* **4**, 53 (1932).
6. H. van Loon, J. C. Rogers, *Mon. Weather Rev.* **106**, 296 (1978).
7. J. W. Hurrell, *Science* **269**, 676 (1995).
8. A discussion of the distinction between the NAO and NAM paradigms and the different indices used to represent this phenomenon can be found in J. M. Wallace, *Q. J. R. Meteorol. Soc.* [**126**, 791 (2000)].
9. J. W. Hurrell, H. van Loon, *Clim. Change* **36**, 301 (1997).
10. The daily-mean data used in the analysis are as follows: The NCEP/NCAR Reanalysis [M. E. Kalnay, and co-authors. *Bull. Am. Meteorol. Soc.* **77**, 437 (1996)] provided by the NOAA Climate Diagnostics Center; United States station data from the NOAA National Climatic Data Center; Japanese station data from the NCAR Data Support Section; and wave height data from the National Data Buoy Center. With the exception of Station 47662 in Tokyo, Japan, which is available only through 1989, all station data have a minimum of 90% of all days during January through March 1958–1997. Daily buoy data are available 1981–1997.
11. January through March (JFM) is defined as the first 90 days of each calendar year. During leap years JFM represents 1 January through 30 March.
12. M. P. Baldwin, T. J. Dunkerton, *J. Geophys. Res.* **104**, 30937 (1999).
13. The daily JFM NAM-index is constructed by projecting JFM daily mean anomaly fields of sea-level pressure, 20° to 90°N, onto the signature of the NAM in the month-to-month variability, as documented in (*4*).
14. Blocking involves the formation of quasi-stationary, long-lived (>7 days), closed anticyclonic circulation cells that temporarily divert the prevailing west-to-east flow of air at middle and upper tropospheric levels. Cold air outbreaks often occur downstream of high-latitude blocking anticyclones (*1*).
15. A result is considered significant at the 95% level if the observed difference between the number of events observed under high and low NAM–index conditions can be replicated less than 5% of the time in 10^5 randomized sortings of the NAM index. The sortings are generated by randomizing the order of the 40 winters in the NAM index, but not the order of the days within each 90-day winter season, hence preserving the autocorrelation characteristics of the original time series.
16. I. G. Rigor, R. L. Colony, S. Martin, *J. Clim.* **13**, 896 (2000).
17. H. M. Cullen, P. B. deMenocal, *Int. J. Climatol.* **20**, 853 (2000).
18. The SD of band-pass filtered (3 to 10 day) 500-hPa height emphasizes disturbances with synoptic timescales. Hence, the shading in Fig. 3 is designed to accentuate the stormtracks.
19. This estimate is based on the assumption that minimum temperatures are normally distributed in the full 40-year sample, in the high NAM–index sample, and in the low NAM–index sample. In this case, the fraction of the number of "cold" (<–1.5 SD) events in the high NAM-index sample to the number of events during the low NAM–index sample (or its reciprocal) is directly related to the correlation coefficient between the standardized NAM index and the respective temperature variable. For example, for $r = 0.1$, the mean temperature would average 0.2 SD higher on high-index days than on low-index days. The frequency of occurrence of negative temperature events would correspond to the area under the normal distribution curve beyond –1.6 SD on high-index days and beyond –1.4 SD on low-index days (0.05:0.08) or ~1:1.5. Similarly, $r = 0.25$ yields a ratio of ~1:2.6, and $r = 0.5$ a ratio of ~1:7.
20. J. M. Wallace, H.-H. Hsu, *Tellus* **37**, 478 (1985).
21. The relations in Tables 2 and 3 were re-evaluated using the leading principal component time series of North Atlantic SLP (20°-90°N; 60°W-30°E) as a surrogate for the index of the NAM. In this case, all of the results are of the same sign as those found in Tables 2 and 3; all but six exceed the 95% confidence level on a station-by-station basis.
22. C.-G. Rossby, *J. Mar. Res.* **3**, 38 (1939).
23. D. W. J. Thompson, J. M. Wallace, G. C. Hegerl, *J. Clim.* **13**, 1018 (2000).
24. J. W. Hurrell, *Geophys. Res. Lett* **23**, 665 (1996).
25. M. Latif *et al.*, *J. Geophys. Res.* **103**, 14375 (1998).
26. M. P. Baldwin, T. J. Dunkerton, *Science*, in preparation.
27. D. T. Shindell, R. Miller, G. Schmidt, L. Pandolfo, *Nature*, **399**, 452 (1999).
28. The percentage decrease in the frequency of occurrence of cold events attributable to the shift in the frequency distribution of the NAM-index between the decades 1958–1967 and 1988–1997 is estimated as follows. Let P_i be the probability of occurrence of cold events when the NAM index is in the ith bin of its frequency distribution, estimated on the basis of the full 40-year period of record, and n_i be the number of days assignable to that bin during a specified decade. The expected number of cold events during, say, the 1958–1967 decade is given by:

$$\sum_{i=1}^{m} P_i \cdot n_i^{58-67}$$

and similarly for the 1988–1997 decade. The estimated decrease in the incidence of cold events between the decades 1958–1967 and 1988–1997 depends on how many bins m are used for representing the probability distribution P_i in the summation: the estimate was found to increase as the number of bins m was increased but to level off for $m > 50$. For example, for $m = 3$, the fractional change in the frequency of occurrence of cold events (<−18°C) over Chicago between 1958–1967 and 1988–1997 is as follows:

$$\frac{(P_{low} \cdot n_{low}^{88-97}) + (P_{neutral} \cdot n_{neutral}^{88-97}) + (P_{high} \cdot n_{high}^{88-97})}{(P_{low} \cdot n_{low}^{58-67}) + (P_{neutral} \cdot n_{neutral}^{58-67}) + (P_{high} \cdot n_{high}^{58-67}} =$$

$$\frac{\left(\frac{84}{595} \cdot 44\right) + \left(\frac{217}{2408} \cdot 583\right) + \left(\frac{29}{597} \cdot 273\right)}{\left(\frac{84}{595} \cdot 209\right) + \left(\frac{217}{2408} \cdot 587\right) + \left(\frac{29}{597} \cdot 104\right)} = 0.82$$

which would be interpreted as an 18% reduction. This reduction was found to increase to –31% for $m > \sim 50$. The calculations in Tables 2 and 3 are based on $m = 61$ bins. The percentage decrease in the frequency of occurrence of cold events attributable to global warming during the same period was estimated assuming (i) that the observed +0.33 K difference in JFM-mean, global-mean temperature between the decades 1958–1967 and 1988–1997 [calculated from data described in P. D. Jones, *J. Clim.* **7**, 1794 (1994)] is distributed uniformly over the entire globe and (ii) that this warming impacts the mean but not the shape of the temperature frequency distribution at each station.

29. Minimum temperature data for the United States and Japan and snowfall data for the United State are based on station data. Daily minimum temperature data for Paris, Novosibirsk, and Beijing were derived using 6-hourly data from the NCEP/NCAR Reanalysis, and snowfall data for Paris and Tokyo were derived from the NCEP/NCAR Reanalysis as precipitation days when the daily mean temperature was below 0°C.
30. Buoy 46005 (located off the coast of Washington State at 46°N, 131°W) and Buoy 44005 (located off the coast of New England at 43°N, 69°W). Winds are based on station data.
31. Blocking events are defined as intervals in which 500-hPa height from the NCEP/NCAR Reanalysis exceeds 1 SD about its mean for five consecutive days. The regions listed in Table 2 correspond to those regions where high-latitude blocking is observed to occur most frequently [J. Shukla, K. Mo, *Mon. Weather Rev.* **111**, 388 (1983)].
32. Thanks to M. P. Baldwin, C. S. Bretherton, C. Deser, D. L. Hartmann, M. Hiltner, M. Holmberg, J. Hurrell, N. J. Mantua, and C. F. Mass for their help at various stages of this research and also to the anonymous reviewers for their insightful comments. D.W.J.T. was supported by the NASA Earth System Science Fellowship Program and by funding provided through Colorado State University. J.M.W. was supported by the NSF under Grant 9707069.

11 January 2001; accepted 30 May 2001

Seasonal Modulation of Interseismic Strain Buildup in Northeastern Japan Driven by Snow Loads

Kosuke Heki

Distinct periodic variations with annual frequencies are often found in the time series of continuous Global Positioning System (GPS) site coordinates in northeastern Japan. They show maximum arc-normal contraction of a few millimeters as well as maximum subsidence of 1 to 2 centimeters, both in March. In northeastern Japan, it snows heavily on the western flank of the backbone range, attaining a maximum depth of several meters in March. When observed snow depths were compared with the load distribution estimated from the GPS data, the surface loads caused by the snow were found to be largely responsible for the annual displacement of GPS sites. The snow load modulates secular strain buildup in northeastern Japan due to the Pacific Plate subduction, but its relevance to the seasonal change of earthquake occurrences remains uncertain.

The GPS Earth Observation Network (GEONET), the nationwide continuous GPS array run by the Geographical Survey Institute (GSI), Japan, has been useful as a sensor for secular (*1*) and earthquake-specific (*2, 3*) crustal deformation. These GPS site coordinates often show conspicuous seasonal variations in addition to interseismic secular movements. Recently, Murakami and Miyazaki (*4*) found that the seasonal signals are coherent in phase to a large extent, and their amplitudes are systematic in space. They fixed a station in central Japan (Komatsu, Fig. 1) and showed that the directions of the annual signals relative to Komatsu coincide with the plate convergence at the Japan Trench, and that their amplitudes are larger where secular velocities are faster. These features suggest an unforeseen possibility that the plate velocity or the coupling strength at depth changes annually (i.e., faster subduction or stronger coupling occurs in winter).

Murakami and Miyazaki (*4*) confirmed that the annual signals are consistent for different receiver and antenna types, and for solutions with different software packages with and without the estimation of atmospheric delay gradients (*5*). They further confirmed that similar annual signals exist in the data from the Japanese domestic very long baseline interferometry (VLBI) observations (*6*). Thus, despite the lack of physical explanation for the seasonal variations, they suggested that the signals are real. Here, I investigated whether snow accumulation in northeastern Japan can provide a sufficient surface load to reproduce the necessary elastic deformation of the solid Earth to account for the GPS variations. Such a finding would thus serve as an independent confirmation of the reality of the signal.

Daily solutions of the GEONET GPS site coordinates relative to the central station at Tsukuba, Ibaraki (Fig. 1), were taken from the GSI website (www.gsi.go.jp) for northeastern Japan covering the period 1998.9–2001.0. The data are based on a routine analysis strategy (*7*) of GSI and are essentially of the same quality as the 1996–1999 data used by Murakami and Miyazaki (*4*). They fixed the Komatsu station (Fig. 1) because its secular velocity represents that of the Eurasian Plate. Here, however, I considered pairs of GPS points that represent the western and eastern sides of the island arc, and compared their baseline length time series.

The baselines on the Japan Sea side have large annual components: They shorten by a few millimeters in winter (Fig. 2, B and E), a result consistent with (*4*). On the other hand, seasonal signatures are smaller on the Pacific side of the arc (Fig. 2, A and D) and have the opposite sense (shortening in summer). Such a contrast across the backbone range is seen for most pairs of baselines. If the annual signal reflects changes in the convergence rate or the coupling strength at the Japan Trench, its amplitude would be proportional to the secular shortening rate, irrespective of which side of the arc the baseline lies. Another feature not mentioned in (*4*) is the annual signals in vertical components (Fig. 2, C and F). Most of the sites subside relative to Tsukuba in the winter, and the amplitudes, up to ~2 cm peak-to-peak, are larger along the backbone range than along the coasts. Neither faster subduction nor stronger coupling predicts such a subsidence pattern for the arc. These features make the trench-origin mechanisms untenable.

Four seasons characterize the environment in Japan. In winter, cold and dry air over Siberia becomes humid as it travels across the Japan Sea, leaving heavy snowfalls as it collides with the backbone range of northeastern Japan. Snow mainly falls on the western side of the arc, but the amounts vary from place to place. The deepest snow, seen along the western flank of the backbone range, starts to accumulate in late autumn, reaching a few meters deep in March; it then disappears in May (Fig. 1) except at the highest peaks. Loads on Earth's surface cause subsidence beneath and around these peaks, along with horizontal deformation such that the land shortens beneath the load and extends outside of it. Snow loads distributed along the western half of the arc would cause crustal deformation qualitatively consistent with the GPS baseline data (Fig. 2), arc-normal crustal shortening beneath the snow cover (Fig. 2, B and E), and smaller extension outside the cover (Fig. 2, A and D). It would also cause the subsidence whose maximum lies below the snow load center (Fig. 2, C and F).

Next, I fixed an arbitrary station and modeled each component of the relative position time series of 88 GPS points in northeastern Japan with the linear, annual, and biannual terms (*8*). I discarded 13 sites (*9*) whose root mean squares of the post-fit residuals exceeded 4 mm (horizontal) or 15 mm (vertical). Then I obtained instanta-

Division of Earth Rotation, National Astronomical Observatory, 2-12 Hoshigaoka, Mizusawa, Iwate 023-0861, Japan. E-mail: heki@miz.nao.ac.jp